Michael P. Marks, MD • Norbert J. Pelc, ScD • Michael R. Ross, MD • Dieter R. Enzmann, MD

# Determination of Cerebral Blood Flow with a Phase-Contrast Cine MR Imaging Technique: Evaluation of Normal Subjects and Patients with Arteriovenous Malformations[1]

**This study evaluated a phase-contrast cine magnetic resonance (MR) imaging technique capable of simultaneously allowing determination of velocity and volume flow rate (VFR) in both carotid arteries and the basilar artery. Forty patients were studied; 24 were neurologically normal, and 16 had intracerebral arteriovenous malformations (AVMs). In the normal group, mean basilar flow was significantly less than mean carotid flow. Mean velocity and VFR showed a significant decline with age in the basilar artery. Carotid artery flow and total cerebral blood flow did not decline with age. In the AVM patients, flow and velocity measurements were significantly elevated in all three arteries. Flow in the carotid artery ipsilateral to the AVM was significantly greater than flow in the contralateral carotid artery. VFR increased in all three arteries with increasing AVM volume. Four patients underwent partial embolization, and a corresponding decrease in flow was observed. Phase-contrast cine MR imaging provides rapid, simultaneous, noninvasive velocity and VFR measurement in the major intracranial arteries.**

**Index terms:** Arteriovenous malformations, cerebral, 10.1494 • Blood, flow dynamics • Blood vessels, MR, 1723.1214, 1753.1214 • Brain, MR, 1723.1214, 1753.1214 • Magnetic resonance (MR), vascular studies

**Radiology 1992;** 182:467–476

THERE is presently no technique available that can allow routine evaluation of cerebral blood flow (CBF) in the major intracranial vessels or determination of global CBF. The velocity of flowing blood can be determined with Doppler ultrasound (US) and applied to intracranial arteries by using transcranial acoustic windows (1,2). Doppler US is limited to evaluation of blood velocity (in centimeters per second) and at present is unable to give an accurate assessment of the volume flow rate (VFR) through an artery (3). A technique that could accurately measure VFR (in milliliters per minute) in major intracranial arteries would provide more critical physiologic information regarding blood flow to the brain in normal and disease states.

Magnetic resonance (MR) imaging has been applied to measurement of blood flow by using time-of-flight phenomena and phase-contrast techniques (4–7). Phase-contrast methods exploit the fact that moving spins accumulate different transverse phase when moving in the direction of a magnetic field gradient. The phase shift is proportional to velocity, and the proportionality constant is easily controlled. As a result, these techniques are ideally suited to quantitative applications.

Arteriovenous malformations (AVMs) of the brain are congenital lesions that result in abnormal shunting of blood from the arterial to the venous circulation, bypassing the normal capillary network of the brain (8,9). This abnormal shunting of blood bypasses the relatively high-resistance capillary bed of the brain parenchyma surrounding the AVM. This phenomenon has been labeled "steal" (9,10). Cerebral steal may result in symptoms of progressive neurologic dysfunction, neuropsychologic deterioration, and seizures (11,12).

Various methods have been used to evaluate flow changes in the brain surrounding AVMs, including stable xenon computed tomography (CT), radioisotope CBF determination, and single photon emission CT (13–16). These techniques have all shown a decline in CBF in the parenchyma surrounding the AVM. They have not, however, been able to allow determination of absolute values of decreased flow that explain symptoms of steal. Transcranial Doppler US has shown increased velocities in major intracranial arteries supplying AVMs (17), but it has not been possible to quantitate flow, owing to the limitations of this modality.

This study was undertaken to evaluate the use of a phase-contrast cine MR imaging technique for assessment of velocity (in centimeters per second) and blood flow (in milliliters per minute) in major intracranial arteries. The first part of this study concerned healthy adult patients of varying age. The second part of this investigation studied flow-related changes in arteries feeding intracranial AVMs.

## SUBJECTS AND METHODS

### Normal Subjects

Twenty-four adult subjects (17 men and seven women) of varying ages (range, 27–82 years; mean, 44 years) were studied. Female subjects ranged in age from 27 to 82 years (mean, 49 years), and male subjects ranged in age from 29 to 79 years (mean, 42 years). Fourteen subjects were healthy volunteers. Ten patients had undergone diagnostic MR imaging studies as outpatients for problems unrelated to ischemic disease. The studies were performed in these patients to rule out acoustic neuroma or pituitary adenoma or to evaluate

[1] From the Department of Diagnostic Radiology, Stanford University Medical Center, 300 Pasteur Dr, Stanford, CA 94305. Received April 1, 1991; revision requested May 3; revision received August 22; accepted September 4. **Address reprint requests to** M.P.M.



**Abbreviations:** AVM = arteriovenous malformation, CBF = cerebral blood flow, MV = mean velocity, PSV = peak systolic velocity, rCBF = regional CBF, TCBF = total CBF, VFR = volume flow rate.

for trigeminal neuralgia. Patients were not included in the study if they had a medical history suggesting possible ischemic disease (stroke, transient ischemic attacks, dementia, etc). In addition, patients were excluded if they had a history of diabetes mellitus, hypertension, or heart disease.

The subjects were studied with a 1.5-T superconducting imager (Signa; GE Medical Systems, Milwaukee). All subjects underwent initial MR studies of the brain with routine spin-echo axial imaging. These were performed as gated studies (repetition time, >2,000 msec; echo time, 20, 80 msec; one excitation). Images were evaluated for evidence of ischemic disease. Only those subjects with normal studies or with minimal white matter changes (a few small [1–2-mm-diameter] foci in the subcortical white matter) were included in the study. Patients were not included if there were larger foci, many foci, or regions of periventricular white matter involvement. Four of the seven patients older than 50 years had these minimal white matter changes, and none of the patients under 50 years had any white matter changes. An axial section was selected (from the spin-echo series) that allowed for simultaneous evaluation of the velocities and VFRs in both internal carotid arteries and the basilar artery. The evaluation was performed through the vertical precavernous portion of the internal carotid artery and the distal portion of the basilar artery. This imaging plane permitted the arteries to be evaluated as they passed transversely through the plane of measurement without causing significant obliquity to that plane.

## AVM Patients

Sixteen patients with intracerebral AVMs, ranging in age from 13 to 64 years (mean, 37 years), were evaluated in a similar manner. Only one patient in this group was under the age of 18 years. After performance of routine spin-echo imaging as outlined above, an axial plane was selected that allowed for simultaneous determination of the flows in both carotid arteries and the basilar artery. AVM patients were excluded from the study if they had undergone treatment with either surgery or embolization. Four patients in this series were treated with partial embolization and evaluated before and after treatment to determine the effect of partial embolization on blood flow. All embolization procedures were performed by means of superselective catheterization with microcatheters and *n*-butyl cyanoacrylate (Avacryl; Tri-Point Medical, Raleigh, NC).

In addition, all patients underwent biplane angiographic evaluation. These results were correlated with velocity and VFR data obtained with phase-contrast cine MR imaging to exclude anomalies of arterial supply or major stenosis of extracranial or intracranial vessels. For purposes of data analysis, the carotid arteries were considered either ipsilateral or contralateral to the AVM, depending on which hemisphere the AVM occupied at MR imaging. The angiogram was used to determine vascular supply to the nidus of the AVM. In two patients, the AVM nidus did not fill via either right or left carotid injection. All 16 patients showed filling of the AVM from the basilar artery at angiography. For data analysis, comparison between ipsilateral and contralateral carotid arteries did not include the two cases in which neither carotid artery supplied the AVM. Therefore, in the 16 cases evaluated, 14 sets of carotid arteries were compared.

The volume of the AVM nidus was determined with MR imaging supplemented by angiography. A diameter was established in three planes of measurement (anteroposterior, mediolateral, and craniocaudal). The three diameter measurements were averaged and used to calculate the AVM nidus volume by applying the formula for a sphere.

## Phase-Contrast Cine Technique

Phase-contrast cine MR images (18,19) were then obtained. In this variant of cine MR imaging (20), acquisitions with two sequence types are rapidly interleaved. The two sequence types interrogate the same section but have different gradient first moments in the section-select direction. The amount by which the first moment is altered controls the flow sensitivity. In our study, the moment was altered so that a velocity of 150 cm/sec produced a phase shift of 180°. The gradient waveform in the readout direction was first-order moment nulled. The difference in phase between the two complex images at each point in the cardiac cycle provided a spatial map of velocity in the section-select direction; these velocity-encoded images were used for quantitation. Additional imaging parameters were as follows: repetition time, 54 msec; echo time, 9.7 msec; two excitations; flip angle, 30°; 256 × 128 matrix; field of view, 12 cm; and section thickness, 5 mm. Phase encoding was incremented by each cardiac cycle. The data were retrospectively segregated into 16 images per cardiac cycle by using linear interpolation. Complex reconstruction of these data was then performed to produce two complex images for each of the 16 temporal frames. The average of the two magnitude images was retained. These images are comparable with conventional cine MR images and depict anatomic detail (Fig 1a). The other image is a velocity-encoded image in which pixel intensity is directly proportional to velocity, with static structures being gray, white indicating flow in one direction, and black representing flow in the opposite direction. Images equal to the product of magnitude and velocity are displayed (Fig 1b) to suppress noise in regions of low signal intensity.

## Quantitative Method

The value in each pixel of each frame of the velocity-encoded image represents the average velocity of flow in that pixel (in centimeters per second). When the pixel (in centimeters per second) is multiplied by the pixel area (in centimeters squared), the VFR (in milliliters per second) through that pixel in that frame is obtained. Summation of such values within a region that contains a blood vessel yields the total VFR (in milliliters per minute) through the vessel at that point in the cardiac cycle, and the average VFR throughout the cardiac cycle can then be easily calculated (Fig 2).

The quantitative accuracy of phase-contrast measurements of velocity and VFR has been validated (21–23). Kondo et al (23) obtained excellent agreement be-

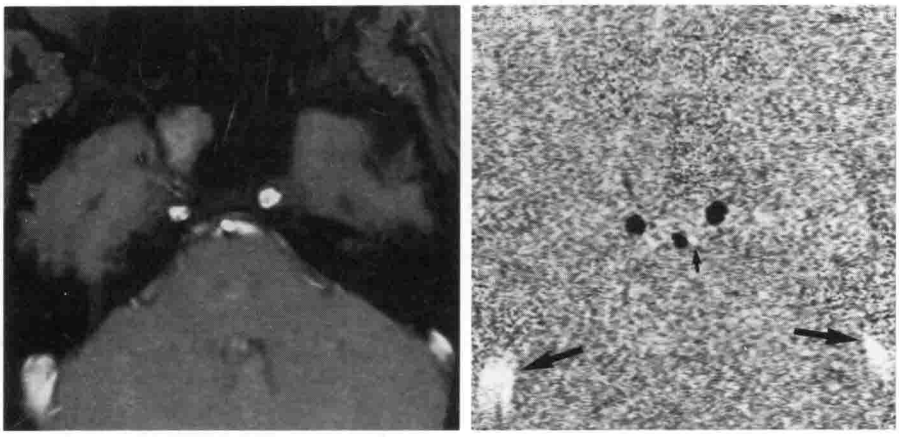

a. b.

**Figure 1.** Magnitude **(a)** and phase-contrast **(b)** images. Axial section allows for simultaneous measurement of flow in both carotid arteries and the basilar artery. On the magnitude image **(a)**, areas of high signal intensity correspond to regions of flow. On the phase-contrast image **(b)**, black areas correspond to flow in the cranial direction as seen in the two carotid arteries and the basilar artery and white areas (large arrows) correspond to flow in the caudal direction as seen in the region of the sigmoid sinus. Note small white area (small arrow) adjacent to the basilar artery; this represents cerebrospinal fluid flowing in a caudal direction during systole.

tween this method and continuous-wave Doppler US in measurement of flow velocity and volume rate in pulmonary arteries. In vitro validation has also been performed (21,22), and it has been shown that the VFR estimate is not significantly altered with vessel obliquity, as the decrease in apparent average velocity is canceled by the increase in vessel area (22).

For vascular measurements, a region of interest was defined for each of the vessels at peak systole in the cardiac cycle. One potential source of error in phase-contrast flow measurements is undesired phase shifts due to eddy currents in the magnetic field. These errors may vary across an image. We corrected for such possible errors by measuring the apparent velocity in static regions immediately adjacent to each vessel. This baseline measurement was subtracted from vessel measurements before any other processing was done.

**Table 1**
**Mean Velocities and VFRs in Normal Subjects**

| Artery | VFR (mL/min) | MV (cm/sec) | PSV (cm/sec) |
|---|---|---|---|
| Right carotid | 352 ± 21 | 46 ± 4 | 63 ± 4 |
| Left carotid | 342 ± 15 | 46 ± 4 | 60 ± 3 |
| Basilar | 164 ± 12 | 40 ± 3 | 51 ± 4 |

## Data Analysis

For each artery evaluated by means of a region of interest, determination of velocity (in centimeters per second) and VFR (in milliliters per minute) during the cardiac cycle was achieved. For each patient, the peak systolic velocity (PSV), mean velocity (MV), and VFR were determined for each of the three arteries. MV was a temporal and spatial average calculated as the MV across the entire lumen of the vessel from 16 phases of the cardiac cycle. Side-to-side variation in MV and VFR between the two carotid arteries was expressed for the right carotid artery as a percentage of the value of the left carotid artery ([right/left] × 100%).

Differences in VFR and velocity values for the two carotid arteries and the basilar artery were compared with the Student *t* test. Statistical analysis of the data with respect to age (in typical subjects) and AVM volume was performed with simple regression analysis and the *t* test. Mean flow and velocity values are given as ± the standard error of the mean unless otherwise indicated.

## RESULTS

### Normal Subjects

The mean values for VFR, MV, and PSV for the normal subject group are shown in Table 1. In the carotid arteries, VFR had a range of 200–666 mL/min. The range in the right carotid artery was 200–666 mL/min, and it was 204–458 mL/min in the left carotid artery. Side-to-side ratios in flow ([right/left] × 100%) varied from 63.9% to 160.9% (mean, 104.3% ± 23.7% [standard deviation]). There was no significant difference in VFR between the right and left carotid arteries in this study. In 11 subjects the VFR was greater in the right artery, and in 13 it was greater in the left. The range of VFR in the basilar artery was 31–280 mL/min. Flow in the basilar artery was significantly less than that observed in either carotid artery ($P < .01$).

The MV range in the right carotid artery was 30–70 cm/sec, and in the left carotid artery it was 31–71 cm/sec. No significant difference in MV was observed between them. In 12 subjects the MV was greater in the right artery, and in 12 it was greater in the left. The side-to-side ratio ([right/left] × 100%) was 77.9%–171.2% (mean, 100.5% ± 20.9% [standard deviation]). Carotid artery velocities were generally higher than those in the basilar artery, and this difference was of borderline significance ($P = .052$). The MV range in the basilar artery was 13–75 cm/sec.

Both velocity and flow were compared with subject age. Flows in the carotid and basilar arteries as a function of age are shown graphically in Figure 3. No significant age-related change was observed for the carotid

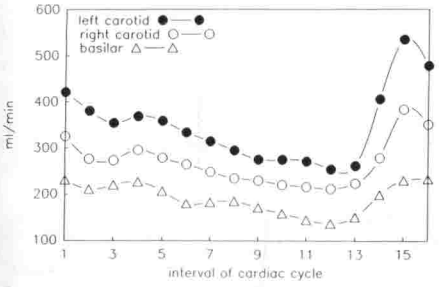


2.

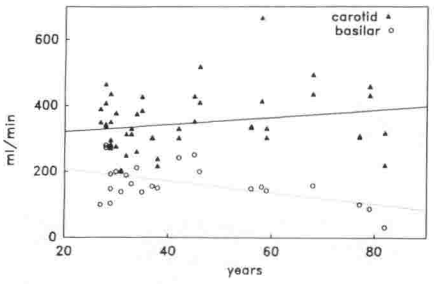


3.

**Figures 2, 3.** **(2)** Diagram of flow rate (in milliliters per minute) versus relative time in the cardiac cycle in a typical normal subject. **(3)** Diagram of carotid and basilar artery VFR (in milliliters per minute) versus age (in years). Basilar artery linear regression: $y = 242.32 - 1.767x$, $r = .524$ ($P = .004$ [one-sided *t* test]). Carotid artery linear regression: $y = 298.92 + 1.096x$, $r = .216$ (difference not significant).

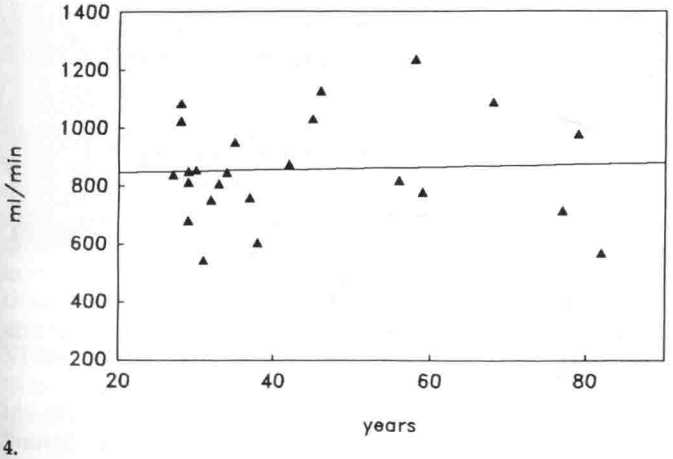


4.

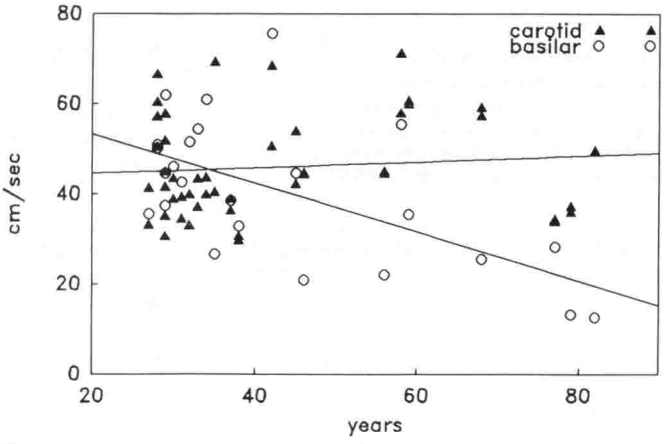


5.

**Figures 4, 5.** **(4)** Diagram of TCBF (in milliliters per minute) versus age (in years). Linear regression: $y = 838.98 + 0.44340x$, $r = .0442$ (difference not significant). **(5)** Diagram of carotid and basilar artery MVs (in centimeters per second) versus age (in years). Basilar artery linear regression: $y = 64.21 - 0.544x$, $r = .606$ ($P < .01$). Carotid artery linear regression: $y = 43.34 - 0.064x$, $r = .101$ (difference not significant).

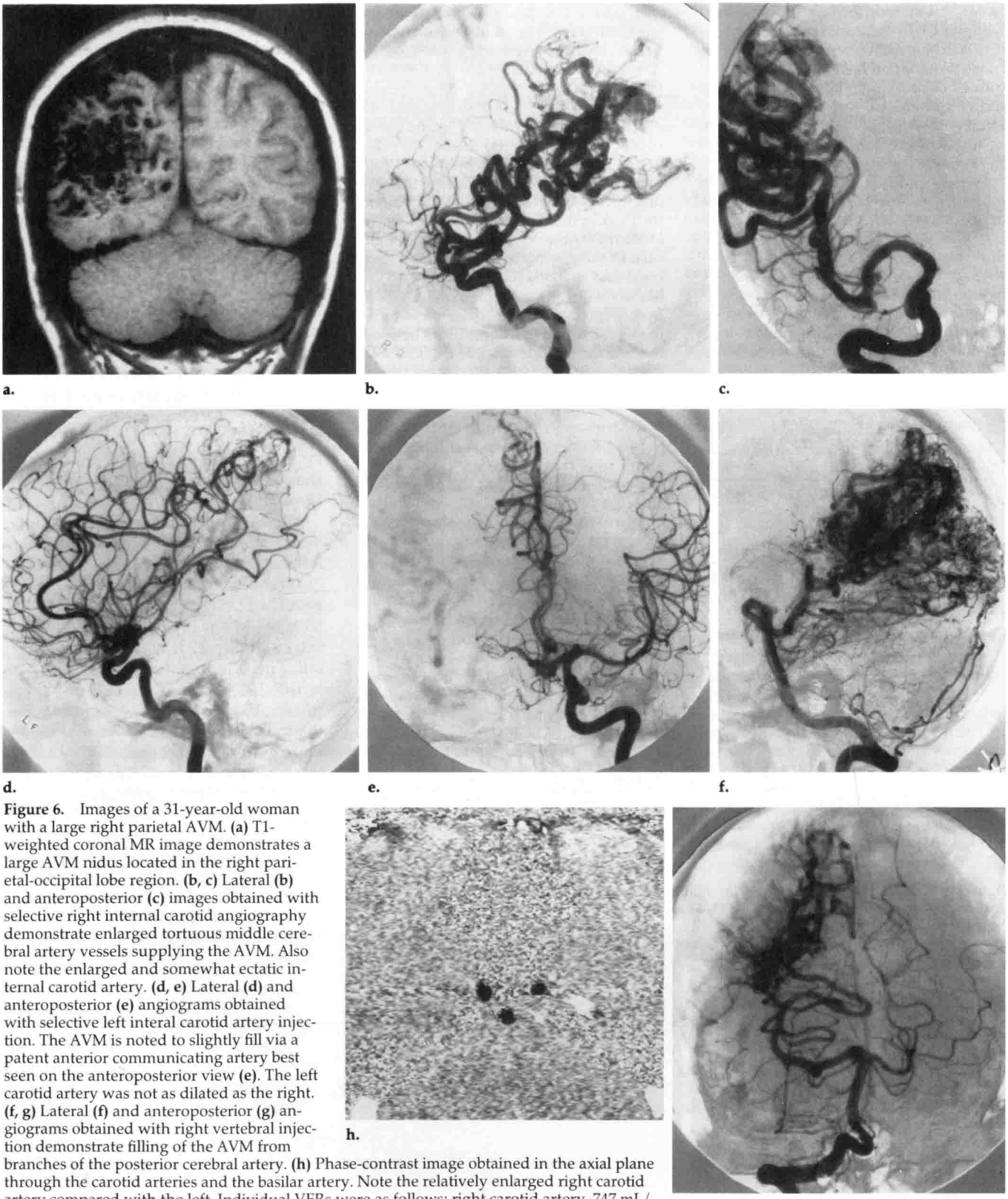


**Figure 6.** Images of a 31-year-old woman with a large right parietal AVM. **(a)** T1-weighted coronal MR image demonstrates a large AVM nidus located in the right parietal-occipital lobe region. **(b, c)** Lateral **(b)** and anteroposterior **(c)** images obtained with selective right internal carotid angiography demonstrate enlarged tortuous middle cerebral artery vessels supplying the AVM. Also note the enlarged and somewhat ectatic internal carotid artery. **(d, e)** Lateral **(d)** and anteroposterior **(e)** angiograms obtained with selective left interal carotid artery injection. The AVM is noted to slightly fill via a patent anterior communicating artery best seen on the anteroposterior view **(e)**. The left carotid artery was not as dilated as the right. **(f, g)** Lateral **(f)** and anteroposterior **(g)** angiograms obtained with right vertebral injection demonstrate filling of the AVM from branches of the posterior cerebral artery. **(h)** Phase-contrast image obtained in the axial plane through the carotid arteries and the basilar artery. Note the relatively enlarged right carotid artery compared with the left. Individual VFRs were as follows: right carotid artery, 747 mL/min; left carotid artery, 423 mL/min; and basilar artery, 701 mL/min.

artery. However, the basilar artery did show a significant age-related decline in flow ($P = .004$ [one-sided $t$ test]).

VFR values in both carotid arteries and the basilar artery were summed for each subject to yield an estimate of total CBF (TCBF). These estimates ranged from 543 to 1,234 mL/min (mean, 858 mL/min ± 36). The TCBF for female subjects was 543–1,083 mL/min (mean, 777 mL/min ± 71), and for male subjects it was 604–1,234 mL/min (mean, 885 mL/min ± 44). TCBF as a function of age is shown in Figure 4. No significant change was observed.

MV was evaluated as it related to age, and this is shown in Figure 5. As a function of age, MV within the carotid arteries did not demonstrate a significant change, but MV within the

**Table 2**
**Velocities and VFRs in AVM Patients**

| Artery | VFR (mL/min) | MV (cm/sec) | PSV (cm/sec) |
|---|---|---|---|
| Ipsilateral carotid* | 563 ± 48 | 90.0 ± 7.8 | 117.2 ± 9.2 |
| Contralateral carotid* | 422 ± 29 | 83.3 ± 7.6 | 111.3 ± 9.7 |
| Basilar† | 385 ± 42 | 83.6 ± 7.2 | 105.3 ± 9.0 |

* $n = 14$.
† $n = 16$.

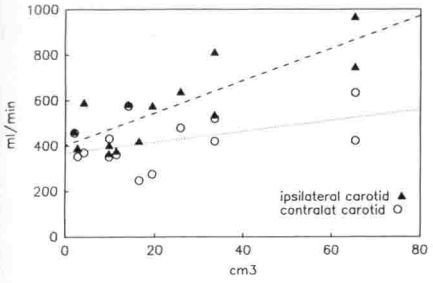


**Figure 7.** Diagram of flow (in milliliters per minute) in carotid arteries ipsilateral and contralateral to the AVM versus AVM nidus volume (in centimeters cubed). Ipsilateral carotid artery linear regression: $y = 403.11 + 7.11x$, $r = .817$ ($P < .01$). Contralateral carotid artery linear regression: $y = 367.50 + 2.41x$, $r = .466$ ($P < .05$).

basilar artery did show a significant decline with age ($P < .01$ [one-sided $t$ test]).

## AVM Patients

The 16 patients evaluated had AVMs in a variety of locations. Five were located in the temporal lobe, four in the parietal lobe, four in the basal ganglia, two in the brain stem, and one in the occipital lobe. The patients presented with a variety of symptoms, including headache, seizures, intracranial hemorrhage, and progressive neurologic deficit.

Figure 6 shows examples of angiograms, an MR image, and a phase-contrast image obtained in a patient with a large parietal AVM. Table 2 gives the mean values obtained for PSV, MV, and VFR in the three vessels evaluated. VFR, PSV, and MV for all arteries in Table 2 were significantly greater than the values obtained for carotid and basilar arteries in normal subjects ($P < .001$). The range of VFR in the ipsilateral carotid artery was 367–968 mL/min, whereas VFR in the contralateral carotid artery ranged from 248 to 635 mL/min. The ipsilateral carotid VFR was found to be significantly higher than the contralateral carotid VFR ($P < .01$). In 13 of 14 patients (93%), ipsilateral carotid flow was greater than contralateral carotid flow. The ratio of ipsilateral-to-contralateral flow varied between 0.93 and 2.10 (mean, 1.36 ± 0.01). Basilar artery VFR varied between 129 and 701 mL/min; this was not significantly different ($P = .055$) from carotid VFR.

AVM nidus volume varied considerably, ranging from 0.1 to 65.4 $cm^3$ (mean, 20.4 $cm^3$ ± 20.3 [standard error]). Figure 7 shows the relationship between carotid VFR and AVM volume. Figure 8 demonstrates basilar VFR versus AVM volume. Linear regression analysis of VFR in all three arteries showed statistically significant slopes, which demonstrated increasing VFR with increasing AVM size. In addition, the linear regression slope for the ipsilateral carotid artery was significantly greater than that for the contralateral carotid artery ($P < .01$). TCBF was obtained by adding the flow values in all three vessels for each patient. The TCBF varied between 615 and 1,947 mL/min (mean, 1,292 ± 93). Figure 9 shows the relationship of TCBF to AVM volume. As with VFR from individual arteries, the TCBF plotted versus AVM size gave a statistically significant positive slope ($P < .01$).

MV ranged from 48.5 to 145.0 cm/sec in the ipsilateral carotid artery. The contralateral carotid artery demonstrated a range of 35.1–139.0 cm/sec. Although the trend was for ipsilateral carotid velocities to be higher than contralateral carotid velocities, this trend was not statistically significant. Basilar artery velocities varied between 43 and 148 cm/sec and were not significantly different from carotid velocities. Linear regression analysis of the MV in the basilar artery showed a significantly positive correlation with AVM size ($P < .05$). The linear regression for both the ipsilateral and the contralateral carotid arteries did not prove statistically significant.

Four patients underwent treatment with partial embolization performed by means of flow-directed microcatheters and $n$-butyl cyanoacrylate. These patients underwent phase-contrast cine MR evaluation before and after treatment. Changes in VFR for these four patients are shown in Table 3. All the patients evaluated showed a considerable reduction in TCBF after treatment. In three of the four patients, flow in all vessels was decreased. One patient (patient 2) showed a considerable decline in basilar artery VFR; however, both carotid arteries (neither of which supplied the AVM) showed an increase in flow after embolization (Fig 10).

# DISCUSSION

## Normal Subjects

The first studies to evaluate CBF used the nitrous oxide technique developed by Kety and Schmidt in 1948 (24). Kety later concluded in a review of data from several groups that a gradual decline in CBF occurred throughout adult life in typical subjects (25). Other contemporary authors using the nitrous oxide technique did not observe an age-related decline in CBF when risk factors for cardiovascular disease were used to select the study population (26). Several authors have used the xenon-133 inhalation (27–32) and stable xenon–CT (33–35) techniques to measure regional CBF (rCBF) changes and have shown a decline in rCBF with advancing age. Similarly, use of positron emission tomography has shown a decline in CBF in some studies (36,37). However, other studies with positron emission tomography have not been able to demonstrate an age-related decline in CBF in normal populations (38,39).

An important factor contributing to the discrepancy in these results may be the criteria used for the selection of normal subjects. Most of the cited studies screened for risk factors for vascular disease (hypertension, diabetes, heart disease, etc). A few used more extensive neuropsychologic testing. Only two groups of investigators used imaging to screen their normal patient population for evidence of ischemic disease (35,38). Itoh et al (38) used CT and excluded patients with brain lesions but retained patients with a "point-like lacuna or mild periventricular hypodensity." Imai et al (35) used neurologically normal volunteers with normal CT scans but included patients with hypertension, diabetes, hyperlipidemia, and heart disease.

MR imaging is more sensitive than CT in the detection of white matter

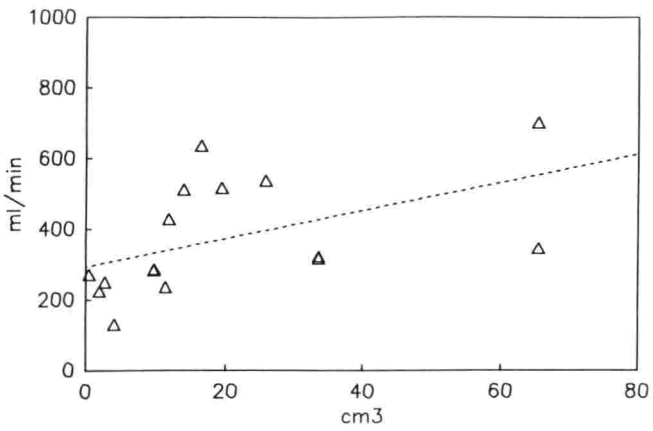


8.

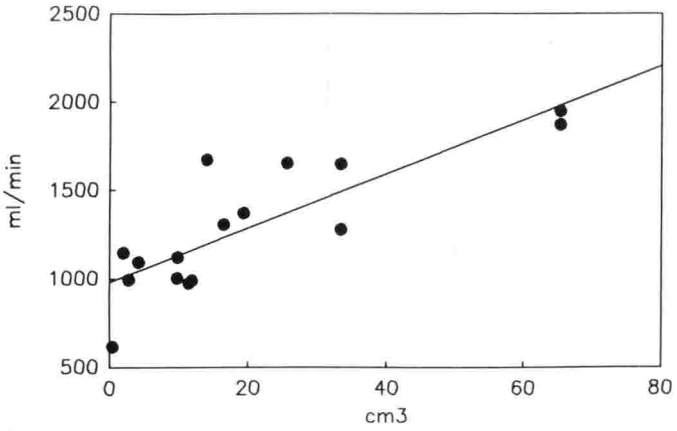


9.

**Figures 8, 9.** **(8)** Diagram of flow (in milliliters per minute) in basilar artery versus AVM nidus volume (in centimeters cubed). Linear regression: $y = 293.34 + 3.98x$, $r = .497$ ($P < .05$). **(9)** Diagram of TCBF (in milliliters per minute) versus AVM nidus volume (in centimeters cubed). Linear regression: $y = 979.15 + 15.334x$, $r = .832$ ($P < .01$).

**Table 3**
**Flow Changes in AVMs after Partial Embolization**

| Patient | AVM Location | Nidus Size ($cm^3$) | Volume Reduction (%) | TCBF (mL/min)* | VFR (cm/sec)* | | |
|---|---|---|---|---|---|---|---|
| | | | | | Ipsilateral Carotid Artery | Contralateral Carotid Artery | Basilar Artery |
| 1 | Left mesencephalic | 4.2 | 80 | 1,091/415 (62) | 591/337 (43) | 370/361 (2) | 130/77 (41) |
| 2 | Left temporal | 12.0 | 80 | 988/887 (10) | . . .† | 281/343 (122) | 428/200 (53) |
| 3 | Right parietal | 65.4 | 20 | 1,870/1,646 (12) | 747/597 (20) | 423/383 (9) | 701/666 (5) |
| 4 | Left parietal | 2.0 | 90 | 1,144/736 (36) | 463/280 (40) | 457/349 (24) | 224/107 (52) |

* Numbers are value before embolization/value after embolization. Numbers in parentheses are percentage of decrease ([value before embolization—value after embolization/value after embolization] × 100%).

† Neither carotid artery supplied the AVM at angiography, so the carotid artery values are averaged in the contralateral category (see Subjects and Methods section).

abnormalities seen as focal regions of high signal intensity in the white matter of the brain on T2-weighted images (40,41). This finding increases in prevalence with age, having been described in 30%–92% of older patients (42–48). Neurologically normal elderly patients show these white matter changes with a prevalence estimated in some studies to be 60% (44,48). Abnormal regions of white matter signal intensity have been found to correlate with cardiovascular risk factors, including heart disease, hypertension, and hyperlipidemia (42). Pathologic evaluation of these lesions has suggested that they are the result of ischemic injury (45,46,49). The deep white matter appears to be more susceptible to ischemic insult because its blood supply is from deeply penetrating arterioles, which are long end arteries without collaterals (50,51). Fazekas et al (52) compared asymptomatic subjects with and without white matter lesions and found that patients with white matter disease had a higher prevalence of extracranial carotid disease and a substantial decrease in white matter CBF.

Our study has demonstrated a statistically significant age-related decline in VFR (in milliliters per minute) in the basilar artery in normal subjects; however, neither carotid flow nor TCBF showed a significant reduction. The data for TCBF in this study group demonstrate a large variation, making it possible that a larger group of subjects would be needed to show a statistically significant decline. However, it is also possible that neurologically normal patients without evidence of ischemic disease at MR imaging maintain the same levels of TCBF throughout life.

Measurement of flow and velocities within intracranial vessels has been difficult. At present, the best noninvasive technique for quantifying velocity is Doppler US. A low-frequency 2-MHz transducer has made it possible to measure flow velocities in the basal cerebral arteries (1). An age-related decline in MVs in these vessels has generally been reported (2,53), but this is not consistently seen (54). A statistically significant decline in MV in the basilar artery was demonstrated with phase-contrast cine MR in this study. No significant change in the carotid arteries or in TCBF could be demonstrated, however.

Since phase-contrast cine MR offers a unique opportunity to measure blood flow (VFR), there is no established standard of reference for these data. We measured a mean value for TCBF of 858 mL/min ± 36. The mean TCBF for female subjects was 777 mL/min ± 71, and it was 885 mL/min ± 44 for male subjects. Assuming a value of 1,354 g for the average weight of the male adult human brain and 1,218 g for that of the female adult brain (55) yields flow values of 65 mL/100 g/min in male subjects and 64 mL/100 g/min in female subjects. These flow values are somewhat higher than those obtained with the nitrous oxide technique (54 mL/100 g/min ± 12 [24]) or with xenon-133 inhalation (56 mL/100 g/min ± 7 [56]). They compare favorably with

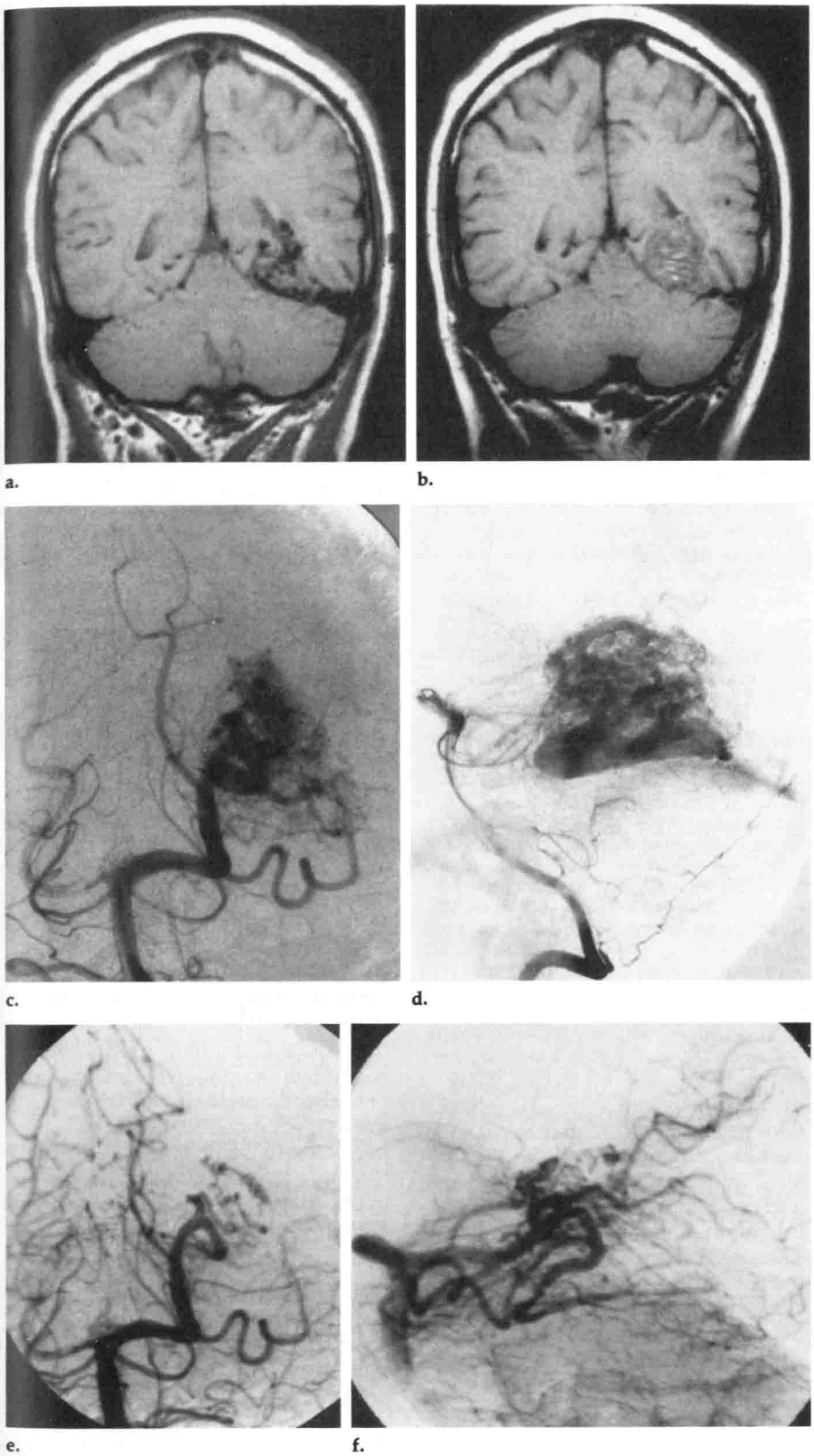


**Figure 10.** Images of a 43-year-old man with a left temporal AVM treated with partial embolization. **(a, b)** T1-weighted MR images obtained in the coronal plane. Pretreatment MR image **(a)** demonstrates the AVM nidus. Posttreatment MR image **(b)** demonstrates replacement of AVM flow voids with areas of intermediate signal intensity after embolization. **(c, d)** Vertebral angiograms obtained in the anteroposterior **(c)** and lateral **(d)** projections before treatment. **(c)** Image obtained during early arterial phase demonstrates filling of the AVM nidus. **(d)** Image obtained slightly later in the arterial phase demonstrates the fully filled AVM nidus with venous drainage. **(e, f)** Anteroposterior **(e)** and lateral **(f)** vertebral angiograms obtained after embolization of two of the major feeding vessels of the AVM nidus and estimated volume reduction of approximately 80%. Flow data before and after embolization are given in Table 3 (patient 2).

rCBF values obtained with xenon CT, which yields flows of approximately 29 and 82 mL/100 g/min for white and gray matter, respectively (57). Our mean flow value of 885 mL/min also compares favorably with flow rates of 879 mL/min ± 55 obtained with labeled erythrocytes (58) and of 839 mL/min ± 226 obtained with jugular venous flow measurement (59). Our technique may slightly overestimate flow, however. The basilar flows are measured at a point that should include the superior cerebellar artery but not other vessels supplying the cerebellum. In the adult, the cerebellum accounts for approximately 10% of the brain weight (60); therefore, this may introduce up to 10% error.

## AVM Patients

Many methods have been used to study the altered hemodynamic state that exists in cerebral AVMs. Early workers evaluated the increased shunt flow resulting from AVMs. In 1948, Shenkin et al used the nitrous oxide technique to demonstrate that ipsilateral and contralateral blood flow through the jugular veins was increased (61). Other workers reported similar results with injected krypton-85 or injected Xe-133 (62,63). Later work has focused on demonstrating decreased blood flow in the parenchyma surrounding the AVM. The AVM nidus consists of small shunting arteries that communicate with large sinusoids or connect directly with veins. This arrangement bypasses the normal intervening high-resistance capillary system (64). This low-resistance AVM shunt has a high rate of blood flow and results in decreased flow in the higher-resistance capillary bed of the normal brain surrounding the nidus. Feindel et al (65) used fluorescein angiography and radioisotopes and demonstrated diminished flow to the brain surrounding AVMs. Similar declines in flow to brain parenchyma near AVMs have been shown by other authors using rCBF determinations obtained with stable xenon CT (13,14,66) and single photon emission CT (16,67). Electrophysiologic studies have shown that neuronal activity is not affected until CBF is decreased to levels below 15 mL/100 g of brain tissue per minute (68). None of these

studies have demonstrated absolute decreases in rCBF that would explain steal symptoms on the basis of inadequate blood supply.

Some of the cited studies have suggested that rCBF is abnormally reduced in areas remote from the AVM, including regions in the opposite hemisphere (14,66,67). Okabe et al demonstrated reductions in rCBF in both hemispheres with use of xenon-CT CBF values, with greater reductions occurring in the ipsilateral hemisphere (66). Our study showed an increase in blood flow in all the major intracranial arteries in patients with AVMs. We also demonstrated that flow in the ipsilateral carotid artery shows a more profound increase compared with contralateral carotid flow.

Stable xenon CT has been used to show that larger AVMs will show a greater decrease in rCBF compared with smaller AVMs (13). Larger AVMs are more likely to cause symptoms of steal (69), since they usually have more shunts. Our study showed a significant correlation between increasing AVM volume and increasing blood flow (in milliliters per minute) in the major intracranial arteries.

The steal phenomenon suggests that there is a maximum flow rate achievable within any of the major intracranial vessels. Beyond this maximum, it is impossible to properly supply the needs of the AVM shunt and the demands of the surrounding brain. This study suggests (from the larger-volume AVMs evaluated) that maximal flow rates are in the range of 800–1,000 mL/min in the carotid artery and approximately 700 mL/min in the basilar artery. A study group with a greater number of large AVMs with high flow rates would be needed to confirm these data. This technique may prove to be a rapid, noninvasive method for evaluating those patients more prone to steal symptoms.

A variety of methods have been used to evaluate rCBF in regions adjacent to AVMs after surgical excision (70–75). These studies all demonstrated that after excision rCBF increases. Petty et al (75)—using transcranial Doppler US—demonstrated a velocity decrease in the basal cerebral arteries after either excision or embolization of AVMs. Our data confirm that in response to partial embolization the velocity and flow in the major intracranial arteries generally decrease. This suggests that partial embolization or excision may be of benefit in the treatment of patients at risk for steal symptoms. However, partially embolized AVMs have been reported to recanalize or develop new anastomotic feeding vessels (76,77), and the more immediate beneficial flow effects may be lost in the long term. Long-term follow-up will be needed to determine if these changes are more permanent.

## Phase-Contrast Technique

The MR phase-contrast method used in this study offers major opportunities for evaluation of blood flow in major intracranial arteries and for determination of TCBF noninvasively. Present techniques for measuring CBF use a variety of methods, including stable xenon CT (57,78), Xe-133 emission CT (56,79), and positron emission tomography (80). All these modalities provide rCBF data. Our technique provides data regarding total flow in individual major blood vessels or global CBF data. It can be argued that cerebral ischemic conditions are better evaluated with a technique that examines focal CBF. However, this technique may provide important information regarding blood flow in major arteries that contributes to these focal changes, such as in carotid occlusive disease.

The dynamic range of this phase-contrast technique is adjustable. As the selected peak-encoded velocity is reduced, the dynamic range of velocities that can be measured decreases and the expected precision improves (81). However, if the time velocity exceeds the selected value, velocity aliasing occurs and the measurement accuracy is degraded. If it occurs, velocity aliasing can be recognized by the appearance of adjacent bright and dark pixels in vessel lumina. With the encoding strength used in this study, aliasing was not observed. Errors can also occur due to the presence of acceleration or higher orders of motion. These effects are minimized by use of the shortest possible echo time. In any case, these higher-order effects do not degrade MV and VFR measurements, since the errors integrate to zero throughout the cycle.

Phase-contrast MR imaging does have some limitations. Partial volume effects are expected to cause overestimation of the flow somewhat, owing to the relatively high signal intensity of moving blood. Similarly, errors can be introduced if the vessels are not significantly larger than the pixel size. These potential sources of error have been reduced through the use of thin sections and small fields of view and are also minimized by choosing appropriate plane orientations.

Inconsistent gating of the temporal sampling can introduce phase variation into the data that appears eventually as artifacts that propagate in the phase-encoding direction if flow is highly pulsatile. These artifacts can be minimized through reduction in the repetition time. Unfortunately, section thickness and pixel size minimization on the one hand, and repetition time minimization on the other, place opposing demands on the system. Nonetheless, further technical improvements can be expected.

In conclusion, a phase-contrast cine MR technique was used to obtain simultaneous measurements of blood flow and blood velocity in both of the internal carotid arteries and the basilar artery. TCBF can be derived from these values. Our results show a significant difference in blood flow between the basilar artery and the carotid arteries. In our normal subjects, there was a significant decline in basilar artery velocity and flow with age, but this was not seen in the carotid artery. TCBF was not changed with age. Additional studies evaluating low-flow states such as those seen in patients with white matter ischemic disease at MR imaging or in patients with fixed stenotic lesions of the major arteries are under way. In AVM patients, flow in the carotid artery ipsilateral to the AVM nidus was found to be significantly greater than that in the contralateral carotid artery. All of the flows increased with increasing AVM volume, suggesting that shunt demand is proportional to AVM size. Evaluation of the effects of partial embolization showed that in the more immediate postembolization period there is a significant flow reduction. Longer follow-up will be needed to determine if these changes are long-standing. ■

### References


1. Aaslid R. Noninvasive transcranial Doppler ultrasound recording of flow in basal cerebral arteries. J Neurosurg 1982; 57:769–774.
2. Arnolds BJ, von Reutern GM. Transcranial Doppler sonography: examination technique and normal reference values. Ultrasound Med Biol 1986; 12:115–123.
3. Taylor KJW, Holland S. Doppler US. I. Basic principles, instrumentation, and pitfalls. Radiology 1990; 174:297–307.
4. Edelman RR, Mattle HP, Kleefield J, Silver MS. Quantification of blood flow with dynamic MR imaging and presaturation bolus tracking. Radiology 1989; 171:551–556.
5. Nayler GL, Firmin DN, Longmore DB. Blood flow imaging by cine magnetic resonance. J Comput Assist Tomogr 1986; 10: 715–722.

6. Bryant DJ, Payne JA, Firmin DN, Longmore DB. Measurement of flow with NMR imaging using a gradient pulse and phase difference technique. J Comput Assist Tomogr 1984; 8:588–593.
7. O'Donnell M. NMR blood flow imaging using multiecho, phase contrast sequences. Med Phys 1985; 12:59–64.
8. Luessenhop AJ. Natural history of cerebral arteriovenous malformations. In: Wilson CB, Stein BM, eds. Intracranial arteriovenous malformations. Baltimore: Williams & Wilkins, 1984; 12–23.
9. Spetzler RF, Selman WR. Pathophysiology of cerebral ischemia accompanying arteriovenous malformations. In: Wilson CB, Stein BM, eds. Intracranial arteriovenous malformations. Baltimore: Williams & Wilkins, 1984; 24–31.
10. Murphy JP. Cerebrovascular disease. Chicago: Year Book Medical, 1954; 242–262.
11. Kusske JA, Kelly WA. Embolization and reduction of the "steal" syndrome in cerebral arteriovenous malformations. J Neurosurg 1974; 40:313–321.
12. Batjer HH, Devous MD, Seibert GB, et al. Intracranial arteriovenous malformation: relationships between clinical and radiographic factors and ipsilateral steal severity. Neurosurgery 1988; 23:322–328.
13. Marks MP, O'Donahue J, Fabricant JI, et al. Cerebral blood flow evaluation of arteriovenous malformations with stable xenon CT. AJNR 1988; 9:1169–1175.
14. Tarr RW, Johnson DW, Rutigliano M, et al. Use of acetazolamide-challenge xenon CT in the assessment of cerebral blood flow dynamics in patients with arteriovenous malformation. AJNR 1990; 11:441–448.
15. Menon D, Weir B. Evaluation of cerebral blood flow in ateriovenous malformations by the xenon 133 inhalation method. Can J Neurol Sci 1979; 6:411–416.
16. Takeuchi S, Kikuchi H, Karasawa J, et al. Cerebral hemodynamics in arteriovenous malformations: evaluation by single-photon emission CT. AJNR 1987; 8:193–197.
17. Lindegaard K-F, Grolinuund P, Aaslid R, Nornes H. Evaluation of cerebral AVMs using transcranial Doppler ultrasound. J Neurosurg 1986; 65:335–344.
18. Pelc NJ, Shimakawa A, Glover GH. Phase contrast cine MRI (abstr). In: Book of abstracts: Society of Magnetic Resonance in Medicine 1989. Berkeley, Calif: Society of Magnetic Resonance in Medicine, 1989; 101.
19. Enzmann DR, Pelc NJ. Normal flow patterns of intracranial and spinal cerebrospinal fluid defined with phase-contrast cine MR imaging. Radiology 1991; 178:467–474.
20. Glover GH, Pelc NJ. A rapid-gated cine MRI technique. Magn Reson Q 1988; 4:299–333.
21. Spritzer CE, Pelc NJ, Lee JN, Evans AJ, Sostman HD, Riederer SJ. Rapid MR imaging of blood flow with a phase-sensitive, limited-flip-angle, gradient recalled pulse sequence: preliminary experience. Radiology 1990; 176:255–262.
22. Rubin DL, Herfkens RJ, Pelc NJ, Jeffrey RB. MR measurement of portal blood flow in chronic liver disease: application to predicting clinical outcome (abstr). In: Book of abstracts: Society of Magnetic Resonance in Medicine 1990. Berkeley, Calif: Society of Magnetic Resonance in Medicine, 1990; 90.
23. Kondo C, Caputo GR, Semelka R, Foster E, Shimakawa A, Higgins CB. Right and left ventricular stroke volume measurements with velocity cine MR imaging. AJR 1991; 157:9–16.
24. Kety SS, Schmidt DF. The nitrous oxide method for the quantitative determination of cerebral blood flow in man: theory, procedure, and normal values. J Clin Invest 1948; 27:476–483.
25. Kety SS. Human cerebral blood flow and oxygen consumption as related to aging. J Chronic Dis 1956; 5:478–486.
26. Shenkin HA, Novak P, Golubff B, Soffe AM, Brotin L. The effects of aging, atherosclerosis, and hypertension upon cerebral circulation. J Clin Invest 1953; 52:459–465.
27. Lavy S, Melamed E, Bentin S, Cooper G, Rinot Y. Bihemispheric decreases of regional cerebral blood flow in dementia: correlation with age-matched normal controls. Ann Neurol 1978; 4:445–450.
28. Meyer JS, Ishihara N, Deshmukh VD, et al. Improved method for noninvasive measurement of regional cerebral blood flow by $^{133}$xenon inhalation. Stroke 1978; 9:195–205.
29. Melamed E, Lavy S, Bentin S, Cooper G, Rinot Y. Reduction in regional cerebral blood flow during normal aging in man. Stroke 1980; 11:31–34.
30. Matsuda H, Maeda T, Masato Y, Gui LX, Tonami N, Hisada K. Age-matched normal values and topographic maps for regional cerebral blood flow measurements by xe-133 inhalation. Stroke 1984; 15:336–342.
31. Shaw TG, Mortel KF, Meyer JS, Rogers RL, Hardenberg J, Cutaia MM. Cerebral blood flow changes in benign aging and cerebrovascular disease. Neurology 1984; 34:855–862.
32. Hagstadius S, Risberg J. Regional cerebral blood flow characteristics and variations with age in resting normal subjects. Brain Cogn 1989; 10:28–43.
33. Tachibana H, Meyer JS, Okayasu H, Kandula P. Changing topographic patterns of human cerebral blood flow with age measured by xenon CT. AJNR 1984; 5:139–146.
34. Amano T, Meyer JS, Okabe T, Shaw T, Mortel KF. Stable xenon CT cerebral blood flow measurements computed by a single compartment–double integration model in normal aging and dementia. J Comput Assist Tomogr 1982; 6:923–932.
35. Imai A, Meyer JS, Kobari M, Ichijo M, Shinohara T, Oravez WT. LCBF values decline while lambda values increase during normal human aging measured by stable xenon-enhanced computed tomography. Neuroradiology 1988; 30:463–472.
36. Pantano P, Baron JC, Lebrun-Grandie P, Duquesnoy N, Bousser MG, Comar D. Regional cerebral blood flow and oxygen consumption in human aging. Stroke 1984; 15:635–641.
37. Leenders KL, Perani D, Lammertsma AA, Heather JD, et al. Cerebral blood flow, blood volume, and oxygen utilization: normal values and effect of age. Brain 1990; 113:27–47.
38. Itoh M, Hatazawa J, Miyazawa H, et al. Stability of cerebral blood flow and oxygen metabolism during normal aging. Gerontology 1990; 36:43–48.
39. Yamaguchi T, Kanno I, Uemura K, et al. Reduction in regional cerebral metabolic rate of oxygen during human aging. Stroke 1986; 17:1220–1228.
40. Braffman BH, Zimmerman RA, Trojanowski JQ, Gonatas NK, Hickey WF, Schlaepfer WW. Brain MR: pathologic correlation with gross and histopathology. II. Hyperintense white matter foci in the elderly. AJNR 1988; 151:559–566.
41. Kobari M, Meyer JS, Ichijo M, Oravez WT. Leukoaraiosis: correlation of MR and CT findings with blood flow, atrophy, and cognition. AJNR 1990; 11:273–281.
42. Awad IA, Spetzler RF, Hodak JA, Awad CA, Carey R. Incidental subcortical lesions identified on magnetic resonance imaging in the elderly. I. Correlation with age and cerebrovascular risk factors. Stroke 1986; 17:1084–1089.
43. Sarpel G, Chaudry F, Hindo W. Magnetic resonance imaging of periventricular hyperintensity in a Veterans Administration hospital population. Arch Neurol 1987; 44: 725–728.
44. Fazekas F, Chawluk JB, Alavi A, Hurtig HI, Zimmerman RA. MR signal abnormalities at 1.5 T in Alzheimer's demential and normal aging. AJNR 1987; 8:421–426.
45. Kirkpatrick JB, Hayman LA. White-matter lesions in MR imaging of clinically healthy brains of elderly subjects: possible pathologic basis. Neuroradiology 1987; 162:509–511.
46. Marshall VG, Bradley WG, Marshall CE, Bhoopat T, Rhodes RH. Deep white matter infarction: correlation of MR imaging and histopathologic findings. Radiology 1988; 167:517–522.
47. Drayer BP. Imaging of the aging brain. I. Normal findings. Radiology 1988; 166:785–796.
48. Hendrie HC, Farlow MR, Austrom MG, Edwards MK, Williams MA. Foci of increased T2 signal intensity on brain MR scans of healthy elderly subjects. AJNR 1989; 10:703–707.
49. Awad IA, Johnson PC, Spetzler RF, Hodak JA. Incidental subcortical lesions identified on magnetic resonance imaging in the elderly. II. Postmortem pathological correlations. Stroke 1986; 17:1090–1097.
50. Reuck JD. The human periventricular arterial blood supply and the anatomy of cerebral infarctions. Eur Neurol 1971; 5:321–334.
51. Reuck JD, Crevits L, De Coster W, Sieben G, vander Eecken H. Pathogenesis of Binswanger chronic progressive subcortical encephalopathy. Neurology 1980; 30:920–928.
52. Fazekas F, Niederkorn K, Schmidt R, et al. White matter signal abnormalities in normal individuals: correlation with carotid ultrasonography, cerebral blood flow measurements, and cerebrovascular risk factors. Stroke 1988; 19:1285–1288.
53. Grolimund P, Seiler RW. Age dependence of the flow velocity in the basal cerebral arteries—a transcranial Doppler ultrasound study. Ultrasound Med Biol 1988; 14:191–198.
54. Hennerici M, Rautenberg W, Sitzer G, Schwartz A. Transcranial Doppler ultrasound for the assessment of intracranial arterial flow velocity—part 1. Surg Neurol 1987; 27:439–448.
55. Ho KC, Roessmann U, Straumfjord JV, Monroe G. Analysis of brain weight. I. Adult brain weight in relation to sex, race, and age. Arch Pathol Lab Med 1980; 104: 635–639.
56. Shirahata N, Henriksen L, Norstrup S, et al. Regional cerebral blood flow assessed by $^{133}$Xe inhalation and emission tomography: normal values. J Comput Assist Tomogr 1985; 9:861–866.
57. Meyer JS, Hayman LA, Amano T, et al. Mapping local blood flow of human brain by CT scanning during stable xenon inhalation. Stroke 1981; 12:426–436.
58. Nylin G, Hedlund S, Rengstrom O. Studies of the cerebral circulation with labeled erythrocytes in healthy man. Circ Res 1961; 9:664–674.
59. Mueller HR, Casty M, Buser M, Haefele M. Ultrasonic jugular venous flow measurement. J Cardiovasc Ultrasonography 1988;

7:25–29.
60. Ellis RS. Norms for some structural changes in the human cerebellum from birth to old age. J Comp Neurol 1920; 32:1–34.
61. Shenkin HA, Spitz EB, Grant FC, Kety SS. Physiologic studies of arteriovenous anomalies of the brain. J Neurosurg 1948; 5:165–172.
62. Lassen NA, Munck O. Cerebral blood flow in arteriovenous anomalies of the brain determined by the use of radioactive krypton 85. Acta Psychiatr Scand 1956; 31: 71–80.
63. Haggendal E, Ingvar DH, Lassen NA, et al. Pre- and postoperative measurements of regional cerebral blood flow in three cases of intracranial arteriovenous aneurysms. J Neurosurg 1965; 22:1–6.
64. Kaplan HA, Aronson SM, Browder EJ. Vascular malformations of the brain. J Neurosurg 1961; 18:630–635.
65. Feindel W, Yamamoto YL, Hcdge CP. Red cerebral veins and the cerebral steal syndrome: evidence from fluorescein angiography and microregional blood flow by radioisotopes during excision of an angioma. J Neurosurg 1971; 35:167–179.
66. Okabe T, Neyer JS, Okayasu H, et al. Xenon-enhanced CT CBF measurement in cerebral AVM's before and after excision: contribution to pathogenesis and treatment. J Neurosurg 1983; 59:21–31.
67. Homan RW, Devous MD, Sokely EM, Bonte FJ. Quantification of intracerebral steal in patients with arteriovenous malformation. Arch Neurol 1986; 43:779–785.
68. Astrup J, Symon L, Branston NM, Lassen WA. Cortical evoked potential and extracellular $K^+$ and $H^+$ at critical levels of brain ischemia. Stroke 1977; 8:51–57.
69. Marks MP, Lane B, Steinberg G, Chang P. Vascular characteristics of intracerebral arteriovenous malformations in patients with clinical steal. AJNR 1991; 12:489–496.
70. Barnett GH, Little JR, Ebrahim ZY, Jones SC, Friel HT. Cerebral circulation during arteriovenous malformation operation. Neurosurgery 1987; 20:836–842.
71. Rosenblum BR, Bonner RF, Oldfield EH. Intraoperative measurement of cortical blood flow adjacent to cerebral AVM using laser Doppler velocimetry. J Neurosurg 1987; 66:396–399.
72. Young WL, Prohovnik I, Ornstein E, et al. Monitoring of intraoperative cerebral hemodynamics before and after arteriovenous malformation resection. Anesth Analg 1988; 67:1011–1014.
73. Young WL, Prohovnik I, Ornstein E, et al. The effect of arteriovenous malformation resection on cerebrovascular reactivity to carbon dioxide. Neurosurgery 1990; 27: 257–267.
74. Batjer HH, Devous MD, Seibert GB, et al. Intracranial arteriovenous malformation: relationships between clinical and radiographic factors and ipsilateral steal severity. Neurosurgery 1988; 23:322–328.
75. Petty GW, Massaro AR, Tatemichi TK, et al. Transcranial Doppler ultrasonographic changes after treatment for arteriovenous malformations. Stroke 1990; 21:260–266.
76. Vinuela F, Fox AJ, Pelz D, Debrun G. Angiographic follow-up of large cerebral AVMs incompletely embolized with isobutyl-2-cyanoacrylate. AJNR 1986; 7:919–925.
77. Berthelsen B, Lofgren J, Svendsen P. Embolization of cerebral arteriovenous malformations with bucrylate. Acta Radiol 1990; 31:13–21.
78. Gur D, Wolfson SK Jr, Yonas H, et al. Progress in cerebrovascular disease: local cerebral blood flow by xenon-enhanced CT. Stroke 1982; 13:750–758.
79. Lassen Niels A. Cerebral blood flow tomography with xenon-133. Semin Nucl Med 1985; 14:347–356.
80. Frackowiak RSJ, Lenzi GL, Jones T, Heather JD. Quantitative measurement of regional cerebral blood flow and oxygen metabolism in man using $^{15}O$ and positron emission tomography: theory, procedure, and normal values. J Comput Assist Tomogr 1980; 6:727–736.
81. Pelc NJ, Bernstein MA, Shimakawa A, Glover GH. Encoding strategies for three-direction phase-contrast MR imaging of flow. JMRI 1991; 1:405–413.